Diagnostics of the ionospheric conductivity based on spacecraft observations of the magnetospheric ULF waves

E. E. Smotrova[1], P. N. Mager[1], O.S. Mikhailova[1], D. Yu. Klimushkin[1]

[1]Institute of Solar-Terrestrial Physics SB RAS, Irkutsk, Russia

Key Points:

- A method for estimating the ionospheric conductivity based on spacecraft observations of Alfvén waves in the magnetosphere is proposed
- The parallel structure of an Alfvén wave under various conditions of the ionospheric conductivity is reconstructed
- The height-integrated Pedersen conductivity of the ionosphere were estimated for the October 27, 2012 event

Corresponding author: E. E. Smotrova, katerina.smotrova@mail.iszf.irk.ru

Abstract

In 27 October 2012 the ULF wave in Pc4 range being Alfvén wave was observed with Van Allen Probe A. In the event the parallel Poynting flux of the wave was directed towards the Northern ionosphere. Assuming that this may be caused by the asymmetry of ionospheric conductivity between the Northern and Southern hemispheres, its effect on the standing structure of the Alfvén wave was investigated in this paper. For this purpose the analytical model with straight magnetic field lines was used. As a result the method for estimation of the Northern and Southern ionospheric conductivity was developed. It allows us to reconstruct the parallel structure of Alfvén waves under various conditions of the ionospheric conductivity. With the method developed, the ionospheric conductivity for the October 27, 2012 event was evaluated and compared with ionosphere model IRI-2016.

Plain Language Summary

The most commonly observed ULF waves in the magnetosphere are Alfvén waves standing along magnetic field line between magnetically conjugated points of the ionosphere located in opposite hemispheres. In this paper we considered how the north-south asymmetry of the ionospheric conductivity influences on standing Alfv́en wave's parallel structure. The model predicts that the structure of the Alfvén waves may differ depending on the conductivity values of Northern and Southern ionospheres. Based on the model we developed the method to carry out a qualitative estimation of the ionospheric height-integrated Pedersen conductivity using parameters of Alfvén waves observed with spacecraft in the magnetosphere. As a result, for the 27 October 2012 event the parallel structure of the observed Alfvén wave was reconstructed and the ionospheric conductivity was estimated. We found a significant difference in the conductivity values of the Northern and Southern ionospheres. The mean is that the magnetically conjugated footprints of spacecraft trajectory, where the event observed, were located on different sides from the line that divides the day side and the night side of Earth (terminator line).

1 Introduction

Studies of the coupled system of ionosphere-magnetosphere is of crucial importance for the plasma processes in the near-Earth's space. An important part of this system is the ultra low frequency (ULF) waves, observed both in space and on the ground. The ULF waves are the field line oscillations with frequencies of the order or lower than the proton gyrofrequency. The most widespread classification categorizes these wave into regular pulsations Pc1–5 ranges (periods from 0.2 to 600 s) and irregular Pi1–2 pulsations (periods from 1 to 150 s) (Jacobs et al., 1964). These waves are interpreted in terms of magnetohydrodynamic (MHD) oscillations. Major part of the ULF waves are identified with the Alfvén waves standing along the field line between the magnetically conjugated points of ionosphere (Dungey, 1954; Radoski, 1967; Chen & Hasegawa, 1974; Southwood, 1974).

Standing Alfvén waves are often used for the diagnostics of the magnetospheric plasma (Troitskaya & Gul'elmi, 1967; Chi & Russell, 2005; Menk & Waters, 2013). Indeed, the Alfvén speed is inversely proportional to square root of the mass density, thus the observed wave's frequency allows one to reproduce plasma density distribution (Berube et al., 2006; Takahashi & Denton, 2007). A number of papers were devoted to calculation of the structure of the standing Alfvén waves with different distributions of density and other magnetospheric parameters (Cummings et al., 1969; Orr & Matthew, 1971; Allan & Knox, 1979a; Leonovich & Mazur, 1993; Ozeke & Mann, 2004; Pilipenko et al., 2005; Degeling et al., 2010; Petrashchuk et al., 2022).

However, there is yet another factor influencing wave's structure and frequency, the ionospheric conductivity. The studies of the influence of the conductivity on the standing Alfvén waves began with works (Scholer, 1970; Inoue, 1973; Maltsev et al., 1974; Hughes, 1974; Hughes & Southwood, 1976). Those papers considered ionosphere as a thin layer, which is justified for the long-period ULF waves (Pi2, Pc4–5). It was shown that the incident wave's magnetic field is reflected from the ionosphere due to the Pedersen conductivity, while the electric field reaches the ground due to the Hall conductivity. Further investigations of the ionosphere-magnetosphere interaction by means of the Alfvén waves were performed in (Alperovich & Fedorov, 1984; Glassmeier, 1984; Hameiri & Kivelson, 1991; Leonovich & Mazur, 1991, 1996; Yoshikawa & Itonaga, 1996; Yoshikawa et al., 2002; Sciffer & Waters, 2002; Cheremnykh & Parnowski, 2006; Erkaev et al., 2006; Waters et al., 2013).

Two limiting cases are worth mentioning. If the conductivity is high, then the wave's electric field equals zero on the ionosphere: $E_{\pm} = 0$, where the "+" and "−" signs refer to the conjugate ionospheres. In this case, the oscillating magnetic field line behave as if fixed in the points of intersection with the ionosphere. This oscillation is usually called the "rigid-end" mode (Cummings et al., 1969; Sinha & Rajaram, 1997).

In the opposite case, the conductivity is very small. In this case, the field aligned derivative of the wave's electric field equals zero on the ionosphere: $(\partial E/\partial l)_{\pm} = 0$, where l is a length along the field line. As a result the field line freely slides on the ionosphere. Such mode is called the "free-end mode" (Newton et al., 1978; Allan & Knox, 1979a). In both cases, between the conjugate ionospheres fit an integer half-waves, the Alfvén waves standing along the field line with no energy flux in this direction.

However, the situation is possible where the conductivities on the Northern and Southern magnetically conjugated points are drastically different. It can be caused by the asymmetry of Pedersen conductivity between the Northern and Southern hemispheres. This situation can occur in the polar ionosphere near the solstices, when one hemisphere is illuminated for a long time and the other is correspondingly in darkness (Glassmeier et al., 1999). In this case, a situation is possible where one end of the field line is fixed, and the other freely slides on the ionosphere. Then between the conjugate ionospheres fit an integer quarter-waves. For the first time, such possibility was mentioned in (Allan & Knox, 1979a). Results of further theoretical studies of the quarter-waves were reported in (Allan & Knox, 1979b; Allan, 1983; Bulusu et al., 2014, 2016). The observational evidences for the quarter-waves were presented in (Allan, 1983; Budnik et al., 1998; Bulusu et al., 2015; Obana et al., 2008, 2015).

The observational manifestations of the Alfvén waves at the asymmetric ionospheres are different from those in the symmetric case. Indeed, the frequency of the leading quarter-wave harmonic approximately two times lower than for the half-wave, there is field aligned energy flux. Thus, the Alfvén waves can be used for diagnostics of the ionosphere (Lee et al., 2004; Ozeke & Mann, 2004; Bulusu et al., 2015; Bulusu et al., 2016; Lysak et al., 2020).

Usually, ionospheric conductivities are determined in several ways. One method is based on the using of the models of the atmosphere, ionosphere and magnetic field with equations derived in (Maeda, 1977). For example, paper (Obana et al., 2015) used the atmosphere model MSISE-90, the ionosphere model IRI 95, and near-Earth geomagnetic field model IGRF 95. In another method the ground based instruments are used. The difficulty here appears in the necessity to use either data of combined observations from different instruments, for example, all sky cameras and riometers (Senior et al., 2008); either, special radar measurement programs and empirical models ought to be used (Ieda et al., 2014). Also, the low-orbital satellite data can be used, like SWARM mission. In the case of single satellite, calculation of the ionospheric conductivity demands using rather

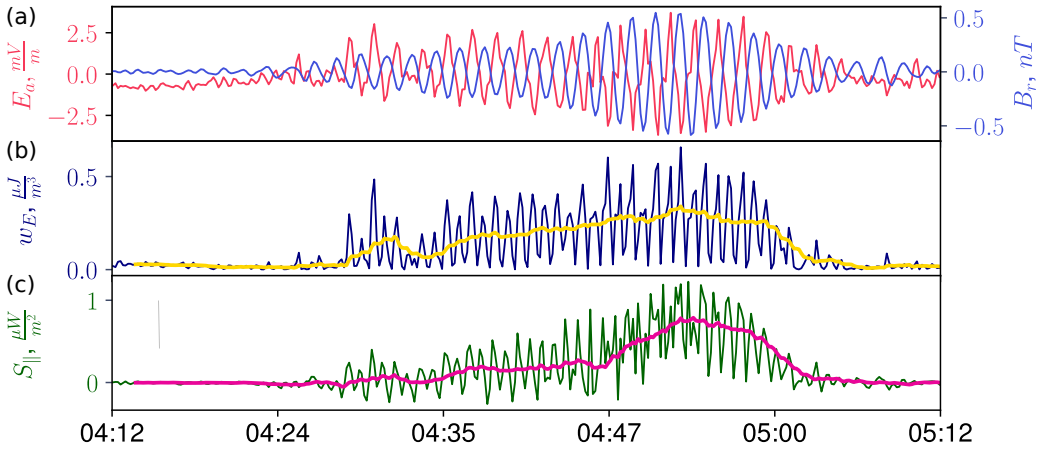

Figure 1. Peculiarities during the 27 October 2012 event: (a) the radial component of the wave's magnetic field B_r (blue line) and the azimuthal component of the wave's electric field E_a (red line); (b) the electric field energy density w_E (dark blue line) and $\overline{w}_E$ (yellow line) averaged over the wave period $T = 100$ c(c) the same for parallel Poynting flux $S_\parallel$ (green line) and $\overline{S}_\parallel$ (red line).

complicated method which give results only along the satellite trajectory (Juusola et al., 2016).

2 27 October 2012 wave event

Let us consider the 27 October 2012 event, in which a poloidal Alfvén wave was observed with The Van Allen Probe A. The wave was registered in the morning part of the magnetosphere at a distance $6.2R_E$. During the event we observed the resonance generation of the ULF wave by the 38 keV electron flux. The electron flux was injected to the magnetosphere due to the substorm. The wave was the fundamental harmonic of the standing Alfvén wave with a frequency 10 mHz and azimuthal wave number $m \approx 110 - 115$. The wave interacted with electrons via the drift resonance and was generated through the gradient instability. The detailed study of the event is presented in (Mikhailova et al., 2022).

We revealed several peculiarities during the 27 October 2012 event studying, which were not mentioned in (Mikhailova et al., 2022). At the figure (Fig. 1) the wave field components, the electric field energy density w_E and the parallel Poynting flux $S_\parallel$, and their values averaged over the wave period $T = 100$ c are presented. One can see that phase shift between the radial component of the wave's magnetic field B_r and the azimuthal component of the wave electric field E_a is about 180°, rather than 90°, as is usually expected for standing waves. Moreover the Poynting flux was directed toward the Northern ionosphere (Fig. 1b). We suggest that these observational peculiarities can be caused by the asymmetry of Pedersen conductivity between the Northern and Southern ionospheres.

3 Principal equations

Let us consider the equation for an Alfvén wave. In the homogeneous background magnetic field and plasma it has a form:

$$\frac{\partial^2 E_j}{\partial l^2} + k_\parallel^2 E_j = 0, \tag{1}$$

where E_j is a component of the wave electric field (under index j is assumed r for the radial component and a for azimuthal one), $k_\parallel = \omega/v_A$ is the parallel component of wave vector, ω is the wave frequency, v_A is the Alfvén speed, l is a coordinate along the magnetic field line. The parallel component of electric field is not considered because it equals to zero in a MHD approximation. We assume the straight magnetic field lines.

The boundary condition for Alfvén waves on the ionosphere were determined in a lot of papers (Hughes, 1974; Hughes & Southwood, 1976; Newton et al., 1978; Leonovich & Mazur, 1991). It can be written in the form

$$E_j|_{l_\pm} = \mp i \frac{\epsilon^\pm}{k_\parallel} \frac{\partial E_j}{\partial l}\bigg|_{l_\pm}, \tag{2}$$

where $l_\pm$ is the coordinate of the Southern (l_-) and Northern (l_+) ionospheric boundaries, the dimensionless parameter $\epsilon^\pm$ is inversely proportional to the height-integrated Pedersen conductivity $\Sigma_P^\pm$,

$$\epsilon^\pm = \frac{c^2}{4\pi \Sigma_P^\pm v_A}, \tag{3}$$

c is the speed of light. Eq. (2) assumes the field to enter to the ionosphere on the normal to it. For more general case, see (Leonovich & Mazur, 1991). The boundary condition (2) determines the damping decrement of the standing Alfvén wave under dissipation in the ionosphere. This one is caused by ionospheric Joule heating at the field line basement (Southwood & Hughes, 1983).

We use the coordinate $l_- = 0$ as a coordinate of the Southern ionosphere boundary and $l_+ = l_I$ as a coordinate of the Northern one. The length of the magnetic filed line l_I can be obtained from the expression

$$l_I = LR_E \int_{-\theta_I}^{\theta_I} \sqrt{1 + 3\sin^2\theta}\cos\theta d\theta, \tag{4}$$

where L is a McIlwain parameter, $\pm\theta_I$ is the geomagnetic latitude of the Southern ($-$) and Northern ($+$) points of intersection of the magnetic field line with the ionosphere. The latitude can be found from the magnetic filed line equation of the dipole magnetic field $r = LR_E\cos^2\theta$, assuming $r = R_E + h_I$, where h_I is height of the upper boundary of the ionosphere (Chapman & Sugiura, 1956).

The dimensionless conductivity parameter $\epsilon^\pm$ (3) let us to take into account different values of Pedersen conductivity at the points of intersection. They are

1. High conductivity of the ionosphere at both the hemispheres: $\epsilon^\pm \ll 1$;
2. Low conductivity of the ionosphere at both the hemispheres: $\epsilon^\pm \gg 1$;
3. Asymmetric conductivity at the different hemispheres: $\epsilon^+ \gg 1, \epsilon^- \ll 1$.

It was assumed at all these cases that the ionospheric conductivities at the different hemispheres have the different absolute value.

The general solution of the wave equation (1) can be represented as

$$E_j = C_1 \exp(ik_\parallel l) + C_2 \exp(-ik_\parallel l). \tag{5}$$

Using boundary condition (2) we found the expression for the coefficients C_1 and C_2, and equation for the parallel wave vector $k_\parallel$:

$$(1-\epsilon^-)(1-\epsilon^+)\exp(ik_\parallel l_I) - (1+\epsilon^-)(1+\epsilon^+)\exp(-ik_\parallel l_I) = 0. \tag{6}$$

To solve (6) let us consider two limiting cases: (i) high conductivity, $\epsilon^\pm \ll 1$; (ii) low conductivity, $\epsilon^\pm \gg 1$. In both cases, the parallel wave vector can be represented in the form

$$k_\parallel = k_0 + \delta k, \quad k_0 = \frac{\pi N}{l_I}, \tag{7}$$

where N is the harmonic wave number, and δk is a small addition caused by small value of $\epsilon^\pm$ in the first case and small value of $(\epsilon^\pm)^{-1}$ in the second case. As result, we found the small value δk and the wave electric field, and, correspondingly, wave magnetic field

$$B_a = -i\frac{c}{\omega}\frac{\partial E_r}{\partial l}, \quad B_r = i\frac{c}{\omega}\frac{\partial E_a}{\partial l} \tag{8}$$

the parallel Poynting flux averaged over the wave period

$$\overline{S}_\parallel = \frac{c}{8\pi}(E_r B_a^* - E_a B_r^*). \tag{9}$$

In the case of high ionospheric conductivity, $\epsilon^\pm \ll 1$, the parallel structure of the wave's electromagnetic field is determined as

$$E_{a,r} = \begin{pmatrix} E_{a0} \\ E_{r0} \end{pmatrix} \left[\sin k_0 l - i\left(\frac{\epsilon^- + \epsilon^+}{l_I} l - \epsilon^-\right)\cos k_0 l\right] \tag{10}$$

$$B_{a,r} = \begin{pmatrix} -B_{a0} \\ B_{r0} \end{pmatrix} \left[\frac{\epsilon^- + \epsilon^+}{k_0 l_I}\cos k_0 l - \left(\frac{\epsilon^- + \epsilon^+}{l_I} l - \epsilon^-\right)\sin k_0 l + i\cos k_0 l\right] \tag{11}$$

where E_{a0} and E_{r0} are the amplitudes of the azimuthal and radial components of the wave electric field, and

$$B_{a0} = E_{r0}\frac{k_0 c}{\omega}, \quad B_{r0} = E_{a0}\frac{k_0 c}{\omega} \tag{12}$$

are the amplitudes of the azimuthal and radial components of the wave magnetic field.

In the opposite low conductivity case, $\epsilon^\pm \gg 1$, the Alfvén wave's parallel structure can be represented as

$$E_{a,r} = \begin{pmatrix} E_{a0} \\ E_{r0} \end{pmatrix} \left[\cos k_0 l - i\left[\left(\frac{1}{\epsilon^-} + \frac{1}{\epsilon^+}\right)\frac{l}{l_I} - \frac{1}{\epsilon^-}\right]\sin k_0 l\right] \tag{13}$$

$$B_{a,r} = \begin{pmatrix} -B_{a0} \\ B_{r0} \end{pmatrix} \left[\left(\frac{1}{\epsilon^-} + \frac{1}{\epsilon^+}\right)\frac{\sin k_0 l}{k_0 l_I} - \left[\left(\frac{1}{\epsilon^-} + \frac{1}{\epsilon^+}\right)\frac{l}{l_I} - \frac{1}{\epsilon^-}\right]\cos k_0 l + i\sin k_0 l\right] \tag{14}$$

For the case of the asymmetric ionosphere (low conductivity of the Northern ionosphere, $\epsilon^+ \gg 1$, and high conductivity of the Southern ionosphere, $\epsilon^- \ll 1$, the parallel wave vector is

$$k_\parallel = \frac{1}{2}k_0 + \delta k \tag{15}$$

the parallel structure is represented as

$$E_{a,r} = \begin{pmatrix} E_{a0} \\ E_{r0} \end{pmatrix} \left[\sin\frac{k_0 l}{2} - i\left[\left(\epsilon^- + \frac{1}{\epsilon^+}\right)\frac{l}{l_I} - \epsilon^-\right]\cos\frac{k_0 l}{2}\right] \tag{16}$$

$$B_{a,r} = \frac{1}{2}\begin{pmatrix} -B_{a0} \\ B_{r0} \end{pmatrix} \left[2\left(\epsilon^- + \frac{1}{\epsilon^+}\right)\frac{\cos\frac{k_0 l}{2}}{k_0 l_N} - \left[\left(\epsilon^- + \frac{1}{\epsilon^+}\right)\frac{l}{l_N} - \epsilon^-\right]\sin\frac{k_0 l}{2} + i\cos\frac{k_0 l}{2}\right] \tag{17}$$

Let us consider properties of the wave's parallel structure on the equator, where $l = l_I/2$. Expressions for the azimuthal component of the wave's electric field E_a, the

radial component of the magnetic field and the parallel Poynting flux $S_\parallel$ are presented in Table 1, where $\Delta\phi$ is the phase shift between B_r and E_a components, and

$$S_0 = \frac{c^2 k_0}{16\pi\omega}(E_{a0}^2 + E_{r0}^2). \tag{18}$$

It is worth to note that only the highest order terms are written.

Table 1. Expressions for the azimuthal component of the wave's electric field E_a, the radial component of the magnetic field and the parallel Poynting flux on the geomagnetic equator for the fundamental harmonic ($N = 1$)

Case	$E_a\left(\frac{l_I}{2}\right)$	$B_r\left(\frac{l_I}{2}\right)$	$\overline{S}_\parallel\left(\frac{l_I}{2}\right)$	$\Delta\phi$
$\epsilon^\pm \ll 1$	E_{a0}	$-\frac{B_{r0}}{2}(\epsilon^+ - \epsilon^-)$	$S_0\left(\epsilon^+ - \epsilon^-\right)$	$\sim 180°, 0°$
$\epsilon^\pm \gg 1$	$-i\frac{E_{a0}}{2}\left(\frac{1}{\epsilon^+} - \frac{1}{\epsilon^-}\right)$	iB_{r0}	$S_0\left(\frac{1}{\epsilon^+} \quad -\frac{1}{\epsilon^-}\right)$	$\sim 180°, 0°$
$\epsilon^+ \gg 1,\ \epsilon^- \ll 1$	$\frac{E_{a0}}{2\sqrt{2}}$	$i\frac{B_{r0}}{2\sqrt{2}}$	$S_0\left[\frac{1}{2}\left(\frac{1}{\epsilon^+} - \epsilon^-\right) - \frac{1}{k_0 l_I}\left(\frac{1}{\epsilon^+} + \epsilon^-\right)\right]$	$\sim 90°$

The following properties of the standing Alfvén wave on the geomagnetic equator are apparent from Table 1:

1. The phase shift between the electric E_a (E_r) and magnetic B_r (B_a) fields for the symmetric conditions is close to 180° or 0°, and for asymmetric conditions to 90°;
2. Since conductivities $\Sigma_P^\pm \propto 1/\epsilon^\pm$, then for the symmetric conditions the absolute value and direction of the parallel Poynting flux $S_\parallel$ is determined by the difference of the ionospheric conductivities ($\epsilon^\pm \gg 1$ case) or their reverse values ($\epsilon^\pm \ll 1$ case).
3. For the asymmetric conditions, the absolute value and direction of the parallel Poynting flux is determined by the combination of the conductivity of one ionosphere and the conductivity reverse value of the other.

The correctness of the results is indicated by the coincidence of the phase shift under symmetric and asymmetric conditions at the boundaries of the ionosphere with early theoretical work (Newton et al., 1978; Southwood & Kivelson, 2001).

4 Ionospheric conductivity estimation model

Expressions received for standing Alfvén wave allow to estimate ionospheric conductivity based on spacecraft data processing of observing magnetospheric Alfvén waves. Inputs include wave parameters such as its period or frequency and wave electric and magnetic field and spacecraft coordinates. Since $v_A = \omega/k_\parallel$ and $k_\parallel \approx k_0 \equiv \pi N/l_I$ for $\epsilon^\pm \ll 1$ and $\epsilon^\pm \gg 1$ symmetric cases, then as follows from eq. (3)

$$\Sigma_P^\pm = \frac{c^2 k_0}{4\pi\omega\epsilon^\pm} = \frac{Nc^2}{4l_I\omega\epsilon^\pm} \tag{19}$$

where the length of magnetic field line l_I can be defined from (4).

With obtained model, the universal method of ionospheric conductivity estimation was developed. It is required to determine ratio between conductivities. For this point, the maximum value of the parallel Poynting flux averaged over the wave period $\overline{S}_\parallel$ is used

(Fig. 1c). Also, the period-averaged energy density of the wave electric or magnetic field

$$\overline{w}_E = \frac{1}{16\pi}(E_r E_r^* + E_a E_a^*), \quad \overline{w}_B = \frac{1}{16\pi}(B_r B_r^* + B_a B_a^*). \tag{20}$$

corresponding to this time is used. For example, as follows from Table 1 for the fundamental harmonic ($N = 1$) at the magnetic equator for $\epsilon^{\pm} \ll 1$ case we have

$$\overline{w}_E = \frac{1}{16\pi}(E_{a0}^2 + E_{r0}^2). \tag{21}$$

and

$$\left(\epsilon^+ - \epsilon^-\right) = \frac{\omega}{c^2 k_0}\frac{\overline{S}_{\parallel}}{\overline{w}_E}. \tag{22}$$

For $\epsilon^{\pm} \gg 1$ case we have

$$\overline{w}_B = \frac{1}{16\pi}(B_{a0}^2 + B_{r0}^2) = \frac{c^2 k_0^2}{16\pi\omega^2}(E_{a0}^2 + E_{r0}^2). \tag{23}$$

and

$$\left(\frac{1}{\epsilon^+} - \frac{1}{\epsilon^-}\right) = \frac{k_0}{\omega}\frac{\overline{S}_{\parallel}}{\overline{w}_B}. \tag{24}$$

If the height-integrated Pedersen conductivity of one ionosphere is known (for example, Southern Σ_P^-), then using the observed values of the period-averaged parallel Poynting flux and energy density the conductivity of the other ionosphere (Northern Σ_P^+) can be calculated with eq. (19) and eq. (22) or eq. (24) depending on the case under consideration

The principle of operation is simple and requires only the availability of the data from magnetospheric observation of Alfvén wave. Moreover, data from one spacecraft is enough for the method to work. Note using method has disadvantage at this stage of development. The fixed height-integrated Pedersen conductivity of one hemisphere is set manually. This can be done using reference theoretical conductivity values or using other empirical models or direct measurements. Thus,the characteristic height-integrated Pedersen conductivity is of order of 10^8 km/s (~ 10 mho) for the daytime ionosphere and 10^7 km/s ($\sim$ 1 mho) for the nighttime ionosphere (Leonovich & Mazur, 1993; Southwood & Hughes, 1983).

Let's obtain criterion for distinguishing cases of high and low ionospheric conductivity ("fixed-end" or "free-end" mode of Alfvén wave). Providing the wave is observed near the geomagnetic equator, the expressions from Table. 1 are valid. For high conductive ionosphere, the difference between the dimensionless values of hemispheres conductivity according to Table. 1 is defined as:

$$\left(\epsilon^+ - \epsilon^-\right) = -\frac{2\omega}{k_0 c}\frac{B_r}{E_a} \tag{25}$$

Since the ionosphere is high conductive medium $\epsilon^{\pm} \ll 1$, the relation between the magnetic and electric field of the observed ULF wave is as follows:

$$\left|\frac{2\omega}{k_0 c}\frac{B_r}{E_a}\right| \ll 1 \tag{26}$$

For the low ionospheric conductivity $\epsilon^{\pm} \gg 1$, the inverse dimensionless values of hemispheres conductivity according to Table. 1 is written as:

$$\left(\frac{1}{\epsilon^+} - \frac{1}{\epsilon^-}\right)^{-1} = -\frac{\omega}{2k_0 c}\frac{B_r}{E_a} \tag{27}$$

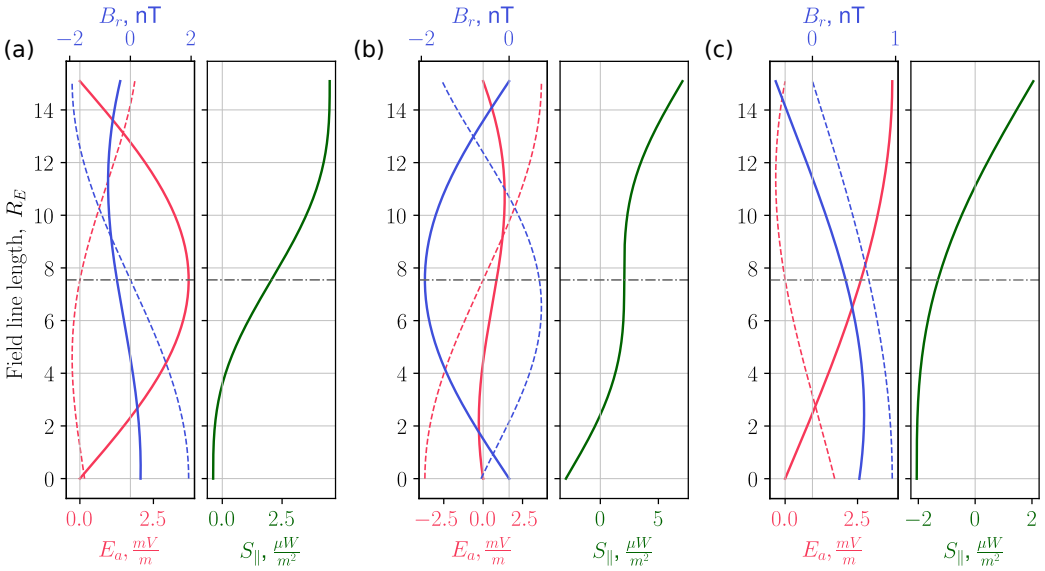

Figure 2. Parallel structure of the Alfvén wave and field aligned Poynting vector component calculated using the ionospheric conductivity estimation model for for the following cases: (a) $\epsilon^{\pm} \ll 1$, (b) $\epsilon^{\pm} \gg 1$, (c) $\epsilon^{+} \gg 1$, $\epsilon^{-} \ll 1$. The solid lines are the real part of calculated values, the dashed lines are the imaginary ones

Then using that fact that the ionosphere is low-conducting $\epsilon^{\pm} \gg 1$, we obtain next result for relation between magnetic and electric fields of the observed wave:

$$\left| \frac{\omega}{2k_0 c} \frac{B_r}{E_a} \right| \gg 1 \tag{28}$$

Criteria (26) and (28) means that the proposed parameter $\epsilon^{\pm}$ should be greater than unity in the case of low conductivity. Otherwise, there is a case of high ionospheric conductivity . The case when proposed criteria equal to unity is not considered due to the fact that the decay decrement will have a value of the order of the wave frequency. It means the wave attenuates very quickly and cannot exist.

5 Estimation ionospheric conductivity during the 27 October 2012 event

The event of 27 October 2012 was observed near geomagnetic equator. Thus, the model proposed in section 4 is applicable for estimation of ionospheric conductivity. Fig. 2 shows an example of how, based on spacecraft data, it is possible to restore the standing structure of the observed wave for different ionosphere conductivity conditions.

Phase shift between radial magnetic field and azimuthal electric field is about 180° for symmetric conditions on ionosphere (Fig.2a,b). Furthermore the case of asymmetric ionospheric conductivity represented on Fig.2c is not suitable because of the peculiarities of the observed wave.

The criteria (26) and (28) were checked for distinguishing symmetric conductivity conditions on the ionosphere. The criterion (26) is met during the observed wave event. In this case one can conclude that ionospheric conductivity was high for both the hemispheres and the almost "fixed-end" mode of the wave was established. Then standing structure of the wave according to the simulation results had the forms as shown in the

Fig. 2a. Besides, we known that the observed wave was in the drift resonance with energetic electrons, and if ionospheric conductivity were low, then the azimuthal electric field of the wave would be asymmetrical and the drift resonance would not be observed.

According to the observational data and equations in Table 1 the difference between dimensionless conductivity parameters for both hemisphere $\epsilon^+ - \epsilon^-$ is equal to 0.476.It is assumed that the difference in the conductivity values may be caused by the fact that the footprints of the spacecraft trajectory, where the event observed, were located on different sides from the terminator line. For verification, the Tsyganenko model T96 (Tsyganenko, 1996) was used to calculate the spacecraft footprints. The terminator line was computed using the Cartopy library of the Python (Met Office, 2010 - 2015). The results are shown in Fig. 3 for the time 04:53 UT when the maximum value of parallel Poynting flux $\overline{S}_{\parallel}$ was registered (Fig. 1a). At that time the spacecraft was located at the magnetic field line corresponding to the magnetic shell $L \approx 6.2 R_E$. Fig. 3 shows that the northern footprint of spacecraft trajectory is located on the night-side ionosphere, and the southern one is on the day-side ionosphere.

As mentioned in section 4 in order to estimate height-integrated Pedersen conductivity the fixed conductivity for one hemisphere is required to set up. In our research, height-integrated Pedersen conductivity in the Southern hemisphere (Σ_P^-) is given by the ionosphere model IRI-2016 (Bilitza et al., 2017). The values of height-integrated Pedersen conductivity is represented in Table 2 based on IRI-2016 model and our method. The order of value of the obtained height-integrated conductivities is consistent with the theoretical estimates from the papers (Southwood & Hughes, 1983; Leonovich & Mazur, 1993) and observational results in (Obana et al., 2008; Ieda et al., 2014; Obana et al., 2015). Dimensionless conductivity parameter for the Northern hemisphere according to the IRI-2016 model is greater than one. Therefore, the observed wave must be the quarter-wave, what means the phase shift between electric and magnetic field of the wave should be around 90°. But according to spacecraft data, this is not observed (Fig. 1a).

Table 2. Height-integrated Pedersen conductivity for the Northern and Southern footprints of the magnetic field line on the 27 October 2012 according to the suggested method at 04:53 UT and the ionosphere model IRI-2016 at 05:00 UT. The last are taken at an altitude of 1000 km above sea

	IRI-2016	Our method
Σ^-, mho (km/s)	9.610 (8.65×10^6)	
ϵ^-	0.043	
Σ^+, mho (km/s)	0.190 (1.71×10^6)	0.795 (7.16×10^6)
ϵ^+	2.172	0.519

There are two factors which can explain difference in the values of height-integrated Pedersen conductivity for Northern hemisphere Σ_P^+. As shown in Fig. 3 the footprints of magnetic field line is located in polar region. In (Bjoland et al., 2016) with compared IRI-2016 model and EISCAT Svalbard radar, it was shown that at the high-latitudes regions model IRI-2016 can underestimate electron density. Another study (Lyakhov et al., 2019) also showed that in transit time (04-08 MLT, from nighttime to daytime), only 25% of calculations based on the IRI-2016 model are within the instrumental accuracy of DE-2 satellite measurements (0±15%).The model IRI-2016 may incorrectly take into

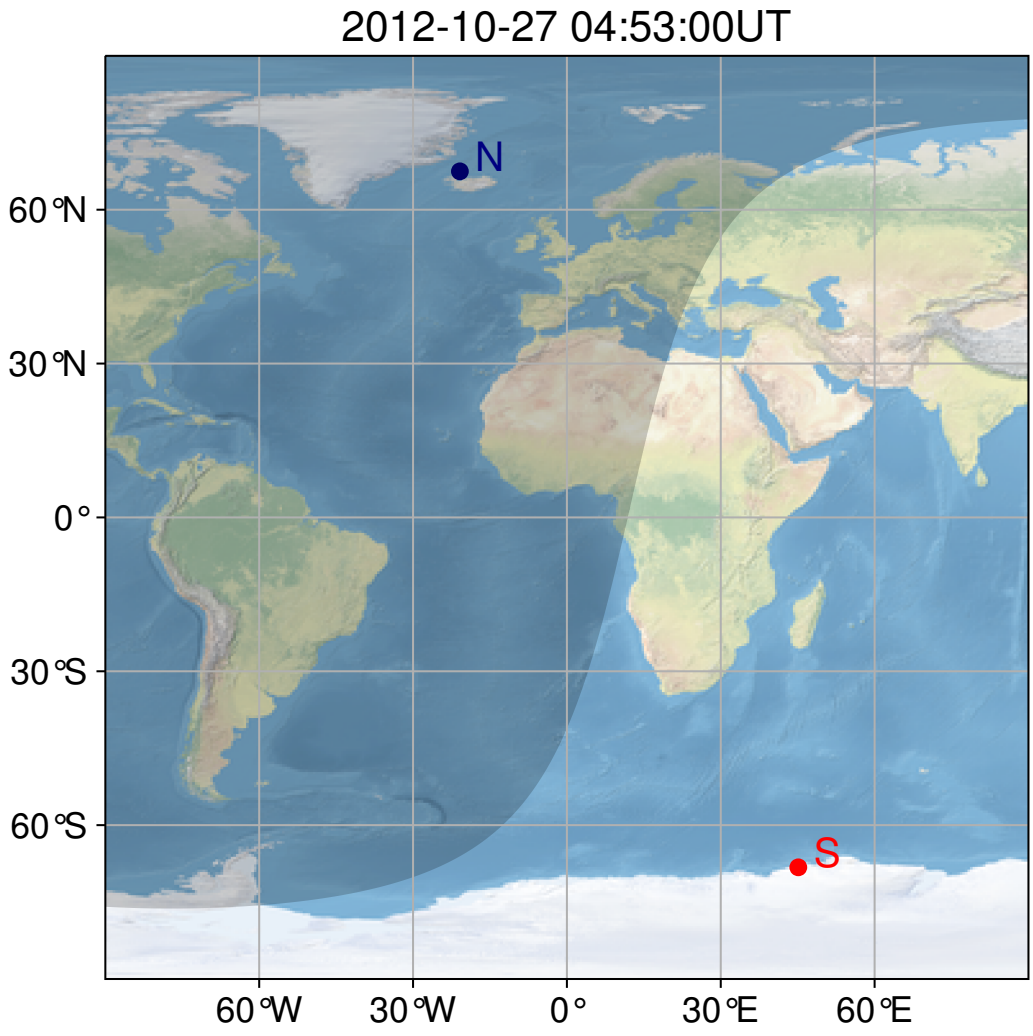

Figure 3. Terminator line and Northern (N) and Southern (S) footprints of the magnetic field line calculated using Tsyganenko model T96 (Tsyganenko, 1996) for the altitude 1000 km above the sea. The terminator and footprints were evaluated from data of event 27 October 2012 at 04:53 UT

account the conditions of the external ionosphere and twilight at all altitudes. Also, it can not properly consider the impact of ionization processes in night side ionosphere.

On the other hand, our proposed method is limited.The use of assumptions that the field enter to the ionosphere on the normal to it, straight magnetic field lines and the requirement of the wave be observed near the geomagnetic equator, influence estimation the relationship between the conductivities. However, the method shows the possibility to use spacecraft data to estimate ionospheric conductivity and their influence on structure of standing Alfvén. The method can be improved by using the dipole model of the magnetic field.

6 Conclusion

The effect of different conductivity of the magnetically conjugated parts of the ionosphere on the structure of standing Alfvén waves using an analytical model with straight magnetic field lines is considered in this paper. Based on the model, a method was developed that allows to estimate the height-integrated Pedersen conductivity at magnetically conjugated points of the ionosphere with spacecraft observations of magnetospheric Alfvén waves. A criterion distinguishing the "fixed-end" and "free-end" of the half-wave mode of the standing Alfvén wave was also obtained from the model. Due to the proposed method, the observational features of the October 27, 2012 event were explained by the difference in conductivity values at the Northern and Southern ionosphere. Proceeding to the criteria, a half-wave mode of the Alfvén wave with almost "fixed-end" at magnetically conjugated points of the ionosphere was proved to be observed for this event. With given Pedersen conductivity for the Southern ionosphere from IRI-2016 model, the conductivity for the Northern ionosphere was estimated. It is shown that the difference in the conductivity values are caused by the fact that footprints of spacecraft trajectory, where the event observed, were located on different sides from the terminator line.

Data Availability Statement

The Van Allen Probes data used in this paper are available at the CDAWeb site (`https://cdaweb.gsfc.nasa.gov/pub/data/rbsp/rbspa/`). The height-integrated Pedersen conductivity data are available at World Data Center for Geomagnetism, Kyoto (`https://wdc.kugi.kyoto-u.ac.jp/ionocond/sigcal/index.html`).

Acknowledgments

The work was financially supported by the Grant of the Russian Science Foundation (project No. 22-77-10032). We acknowledge the NASA Van Allen Probes and Craig Kletzing for use of EMFISIS data, John Wygant for use of EFW data.

References

Bjoland, L., Belyey, V., Løvhaug, U., & La Hoz, C. (2016). An evaluation of International Reference Ionosphere electron density in the polar cap and cusp using EISCAT Svalbard radar measurements. *Annales Geophysicae*, *34*, 751-758. doi: 10.5194/angeo-34-751-2016

Allan, W. (1983). Quarter-wave ulf pulsations. *Planetary and Space Science*, *31*(3), 323-330. doi: 10.1016/0032-0633(83)90083-1

Allan, W., & Knox, F. B. (1979a). A dipole field model for axisymmetric Alfvén waves with finite ionosphere conductivities. *Planetary and Space Science*, *27*(1), 79-85. doi: 10.1016/0032-0633(79)90149-1

Allan, W., & Knox, F. B. (1979b). The effect of finite ionosphere conductivities on axisymmetric toroidal Alfvén wave resonances. *Planetary and Space Science*,

27(7), 939-950. doi: 10.1016/0032-0633(79)90024-2

Alperovich, L. S., & Fedorov, E. N. (1984). Effect of the ionosphere on the propagation of MHD wave beams. *Radiofizika*, *27*(10), 1238-1247.

Berube, D., Moldwin, M. B., & Ahn, M. (2006). Computing magnetospheric mass density from field line resonances in a realistic magnetic field geometry. *Journal of Geophysical Research: Space Physics*, *111*(A8). doi: https://doi.org/10.1029/2005JA011450

Bilitza, D., Altadill, D., Truhlik, V., Shubin, V., Galkin, I., Reinisch, B., & Huang, X. (2017). International Reference Ionosphere 2016: From ionospheric climate to real-time weather predictions. *Space Weather*, *15*, 418-429. doi: 10.1002/2016SW001593

Budnik, F., Stellmacher, M., Glassmeier, K.-H., & Buchert, S. C. (1998). Ionospheric conductance distribution and mhd wave structure: observation and model. *Annales Geophysicae*, *16*(2), 140–147. doi: 10.1007/s00585-998-0140-8

Bulusu, J., Sinha, A. K., & Vichare, G. (2014). Toroidal quarter waves in the Earth's magnetosphere: theoretical studies. *Astrophys. Space Sci.*, *353*, 395-404. doi: 10.1007/s10509-014-2052-2

Bulusu, J., Sinha, A. K., & Vichare, G. (2015). An analytic model of toroidal half-wave oscillations: Implication on plasma density estimates. *Journal of Geophysical Research: Space Physics*, *120*(6), 4164–4180. (2014JA020797) doi: 10.1002/2014JA020797

Bulusu, J., Sinha, A. K., & Vichare, G. (2015). Toroidal quarter waves in the Earth's magnetosphere: observational perspective. *Astrophys. Space Sci.*, *357*(1), 13. doi: 10.1007/s10509-015-2306-7

Bulusu, J., Sinha, A. K., & Vichare, G. (2016). Role of finite ionospheric conductivity on toroidal field line oscillations in the Earth's magnetosphere – Analytic solutions. *Journal of Geophysical Research (Space Physics)*, *121*(6), 5404-5421. doi: 10.1002/2015JA022019

Chapman, S., & Sugiura, M. (1956). Arc-lengths along the lines of force of a magnetic dipole. *Journal of Geophysical Research*, *61*(3), 485–488. doi: 10.1029/jz061i003p00485

Chen, L., & Hasegawa, A. (1974). A theory of long period magnetic pulsation. 1: Steady state excitation of a field line resonance. *Journal of Geophysical Research*, *79*, 1024-1032. doi: 10.1029/JA079i007p01024

Cheremnykh, O. K., & Parnowski, A. S. (2006). Influence of ionospheric conductivity on the ballooning modes in the inner magnetosphere of the Earth. *Advances in Space Research*, *37*(3), 599-603. doi: 10.1016/j.asr.2005.01.073

Chi, P. J., & Russell, C. T. (2005). Travel-time magnetoseismology: Magnetospheric sounding by timing the tremors in space. *Geophysical Research Letters*, *32*(18). doi: https://doi.org/10.1029/2005GL023441

Cummings, W. D., O'Sullivan, R. J., & P. J., C., Jr. (1969). Standing Alfvén waves in the magnetosphere. *Journal of Geophysical Research*, *74*, 778. doi: 10.1029/JA074i003p00778

Degeling, A. W., Rankin, R., Kabin, K., Rae, I. J., & Fenrich, F. R. (2010). Modeling ULF waves in a compressed dipole magnetic field. *Journal of Geophysical Research: Space Physics*, *115*(A10), A10212. doi: 10.1029/2010JA015410

Dungey, J. W. (1954). Electrodynamics of the outer atmospheres. In *Ionospheric science report, no 69* (p. 1-52). Ions. Res. Lab., Pennsylvania State Univ.

Erkaev, N. V., Shaidurov, V. A., Semenov, V. S., Biernat, H. K., & Heidorn, D. (2006). Dissipation of Alfvén wave pulses propagating along dipole magnetic tubes with reflections at the ionosphere. *Advances in Space Research*, *37*(3), 576-580. doi: 10.1016/j.asr.2005.09.002

Glassmeier, K. H. (1984). On the influence of ionospheres with non-uniform conductivity distribution on hydromagnetic waves. *Journal of Geophysics Zeitschrift Geophysik*, *54*(2), 125-137.

Glassmeier, K.-H., Buchert, S., Motschmann, U., Korth, A., & Pedersen, A. (1999). Concerning the generation of geomagnetic giant pulsations by drift-bounce resonance ring current instabilities. *Annales Geophysicae*, *17*, 338–350. doi: 10.1007/s00585-999-0338-4

Hameiri, E., & Kivelson, M. G. (1991). Magnetospheric waves and the atmosphere-ionosphere layer. *Journal of Geophysical Research*, *96*(A12), 21125-21134. doi: 10.1029/91JA02129

Hughes, W. J. (1974). The effect of the atmosphere and ionosphere on long period magnetospheric micropulsations. *Planetary and Space Science*, *22*(8), 1157-1172. doi: 10.1016/0032-0633(74)90001-4

Hughes, W. J., & Southwood, D. J. (1976). The screening of micropulsation signals by the atmosphere and ionosphere. *Journal of Geophysical Research*, *81*, 3234-3240. doi: 10.1029/JA081i019p03234

Ieda, A., Oyama, S., Vanhamäki, H., Fujii, R., Nakamizo, A., Amm, O., ... Nishitani, N. (2014). Approximate forms of daytime ionospheric conductance. *Journal of Geophysical Research: Space Physics*, *119*(12), 10,397-10,415. doi: https://doi.org/10.1002/2014JA020665

Inoue, Y. (1973). Wave polarizations of geomagnetic pulsations observed in high latitudes on the earth's surface. *Journal of Geophysical Research*, *78*(16), 2959-2976. doi: 10.1029/JA078i016p02959

Jacobs, J. A., Kato, Y., Matsushita, S., & Troitskaya, V. A. (1964). Classification of geomagnetic micropulsations. *Journal of Geophysical Research*, *69*(1), 180-181. doi: https://doi.org/10.1029/JZ069i001p00180

Juusola, L., Archer, W. E., Kauristie, K., Burchill, J. K., Vanhamäki, H., & Aikio, A. T. (2016). Ionospheric conductances and currents of a morning sector auroral arc from swarm-a electric and magnetic field measurements. *Geophysical Research Letters*, *43*(22), 11,519-11,527. doi: https://doi.org/10.1002/2016GL070248

Lee, D. H., Kim, K. H., Denton, R. E., & Takahashi, K. (2004). Effects of ionospheric damping on MHD wave mode structure. *Earth, Planets and Space*, *56*, e33-e36. doi: 10.1186/BF03352541

Leonovich, A. S., & Mazur, V. A. (1991). An electromagnetic field, induced in the ionosphere and atmosphere and on the earth's surface by low-frequency Alfven oscillations of the magnetosphere: General theory. *Planetary and Space Science*, *39*(4), 529-546. doi: 10.1016/0032-0633(91)90048-F

Leonovich, A. S., & Mazur, V. A. (1993). A theory of transverse small-scale standing Alfvén waves in an axially symmetric magnetosphere. *Planetary and Space Science*, *41*, 697–717. doi: 10.1016/0032-0633(93)90055-7

Leonovich, A. S., & Mazur, V. A. (1996). Penetration to the Earth's surface of standing Alfvén waves excited by external currents in the ionosphere. *Annales Geophysicae*, *14*, 545-556. doi: 10.1007/s00585-996-0545-1

Lyakhov, A., Kozlov, S., & Bekker, S. (2019). Assessment of the Accuracy of Calculations Using the International Reference Ionosphere Model IRI-2016: I. Electron Densities. *Geomagnetism and Aeronomy*, *59*(1), 45-52. doi: 10.1134/S0016793219010110

Lysak, R. L., Song, Y., Waters, C. L., Sciffer, M. D., & Obana, Y. (2020). Numerical investigations of interhemispheric asymmetry due to ionospheric conductance. *Journal of Geophysical Research: Space Physics*, *125*(7), e2020JA027866. doi: https://doi.org/10.1029/2020JA027866

Maeda, K. (1977). Conductivity and drifts in the ionosphere. *Journal of Atmospheric and Terrestrial Physics*, *39*(9), 1041-1053. doi: 10.1016/0021-9169(77)90013-7

Maltsev, Yu. P., Leontyev, S. V., & Lyatsky, W. B. (1974). Pi-2 pulsations as a result of evolution of an Alfvén impulse originating in the ionosphere during a brightening of aurora. *Planetary and Space Science*, *22*, 1519-1533. doi:

10.1016/0032-0633(74)90017-8

Menk, F. W., & Waters, C. L. (2013). *Magnetoseismology: Ground-based remote sensing of the earth's magnetosphere*. John Wiley and Sons. doi: 10.1002/9783527652051

Met Office. (2010 - 2015). Cartopy: a cartographic python library with a matplotlib interface [Computer software manual]. Exeter, Devon. Retrieved from `https://scitools.org.uk/cartopy`

Mikhailova, O. S., Smotrova, E. E., & Mager, P. N. (2022). Resonant generation of an alfvén wave by a substorm injected electron cloud: A van allen probe case study. *Geophysical Research Letters*, *49*(19), e2022GL100433. doi: 10.1029/2022GL100433

Newton, R., Southwood, D., & Hughes, W. (1978). Damping of geomagnetic pulsations by the ionosphere. *Planet. Space Sci.*, *26*, 201–209.

Obana, Y., Menk, F. W., Sciffer, M. D., & Waters, C. L. (2008). Quarter-wave modes of standing alfvén waves detected by cross-phase analysis. *Journal of Geophysical Research: Space Physics*, *113*(A8). doi: 10.1029/2007JA012917

Obana, Y., Waters, C. L., Sciffer, M. D., Menk, F. W., Lysak, R. L., Shiokawa, K., ... Petersen, T. (2015). Resonance structure and mode transition of quarter-wave ulf pulsations around the dawn terminator. *Journal of Geophysical Research: Space Physics*, *120*(6), 4194-4212. doi: 10.1002/2015JA021096

Orr, D., & Matthew, J. A. D. (1971). The variation of geomagnetic micropulsation periods with latitude and the plasmapause. *Planetary and Space Science*, *19*, 897-905. doi: 10.1016/0032-0633(71)90141-3

Ozeke, L. G., & Mann, I. R. (2004). Modeling the properties of guided poloidal alfvén waves with finite asymmetric ionospheric conductivities in a dipole field. *Journal of Geophysical Research: Space Physics*, *109*(A5). doi: https://doi.org/10.1029/2003JA010151

Petrashchuk, A. V., Klimushkin, D. Y., & Mager, P. N. (2022). Numerical analysis of the spatial structure of Alfvén waves in a finite pressure plasma in a dipole magnetosphere. *Solar-Terrestrial Physics*, *8*, 3-12. doi: 10.12737/stp-83202201

Pilipenko, V. A., Mazur, N. G., Fedorov, E. N., Engebretson, M. J., & Murr, D. L. (2005). Alfvén wave reflection in a curvilinear magnetic field and formation of Alfvénic resonators on open field lines. *Journal of Geophysical Research*, *110*(A9), 10. doi: 10.1029/2004JA010755

Radoski, H. R. (1967). Highly asymmetric MHD resonances. The guided poloidal mode. *Journal of Geophysical Research*, *72*, 4026-4033. doi: 10.1029/JZ072i015p04026

Scholer, M. (1970). On the motion of artificial ion clouds in the magnetosphere. *Planet. Space Sci.*, *18*(7), 977-1004. doi: 10.1016/0032-0633(70)90101-7

Sciffer, M. D., & Waters, C. L. (2002). Propagation of ulf waves through the ionosphere: Analytic solutions for oblique magnetic fields. *Journal of Geophysical Research: Space Physics*, *107*(A10), SIA 11-1-SIA 11-14. doi: 10.1029/2001JA000184

Senior, A., Kosch, M. J., & Honary, F. (2008). Comparison of methods to determine auroral ionospheric conductances using ground-based optical and riometer data. *Annales Geophysicae*, *26*(12), 3831–3840. doi: 10.5194/angeo-26-3831-2008

Sinha, A., & Rajaram, R. (1997). An analytic approach to toroidal eigen mode. *Journal of Geophysical Research: Space Physics*, *102*(A8), 17649-17657.

Southwood, D. J. (1974). Some features of field line resonances in the magnetosphere. *Planetary and Space Science*, *22*, 483-491. doi: 10.1016/0032-0633(74)90078-6

Southwood, D. J., & Hughes, W. J. (1983). Theory of hydromagnetic waves in the magnetosphere. *Space Science Reviews*, *35*(4), 301-366. doi: 10.1007/

BF00169231

Southwood, D. J., & Kivelson, M. G. (2001). Damping standing Alfvén waves in the magnetosphere. *Journal of Geophysical Research Space Physics*, *106*(6), 10829-10836. doi: 10.1029/2000JA000343

Takahashi, K., & Denton, R. E. (2007). Magnetospheric seismology using multiharmonic toroidal waves observed at geosynchronous orbit. *Journal of Geophysical Research*, *112*, A05204. doi: 10.1029/2006JA011709

Troitskaya, V. A., & Gul'elmi, A. V. (1967). Geomagnetic Micropulsations and Diagnostics of the Magnetosphere. *Space Sci. Rev.*, *7*(5-6), 689-768. doi: 10.1007/BF00542894

Tsyganenko, N. A. (1996). Effects of the solar wind conditions in the global magnetospheric configurations as deduced from data-based field models. In (Vol. ESA SP-389, p. 181-185).

Waters, C. L., Lysak, R. L., & Sciffer, M. D. (2013). On the coupling of fast and shear Alfvén wave modes by the ionospheric Hall conductance. *Earth Planets Space*, *65*, 385-396. doi: 10.5047/eps.2012.08.002

Yoshikawa, A., & Itonaga, M. (1996). Reflection of shear Alfvén waves at the ionosphere and the divergent Hall current. *Geophysical Research Letters*, *23*(1), 101-104. doi: 10.1029/95GL03580

Yoshikawa, A., Obana, Y., Shinohara, M., Itonaga, M., & Yumoto, K. (2002). Hall-induced inductive shielding effect on geomagnetic pulsations. *Geophysical Research Letters*, *29*(8), 107-1-107-4. doi: 10.1029/2001GL013610

Figure 1.

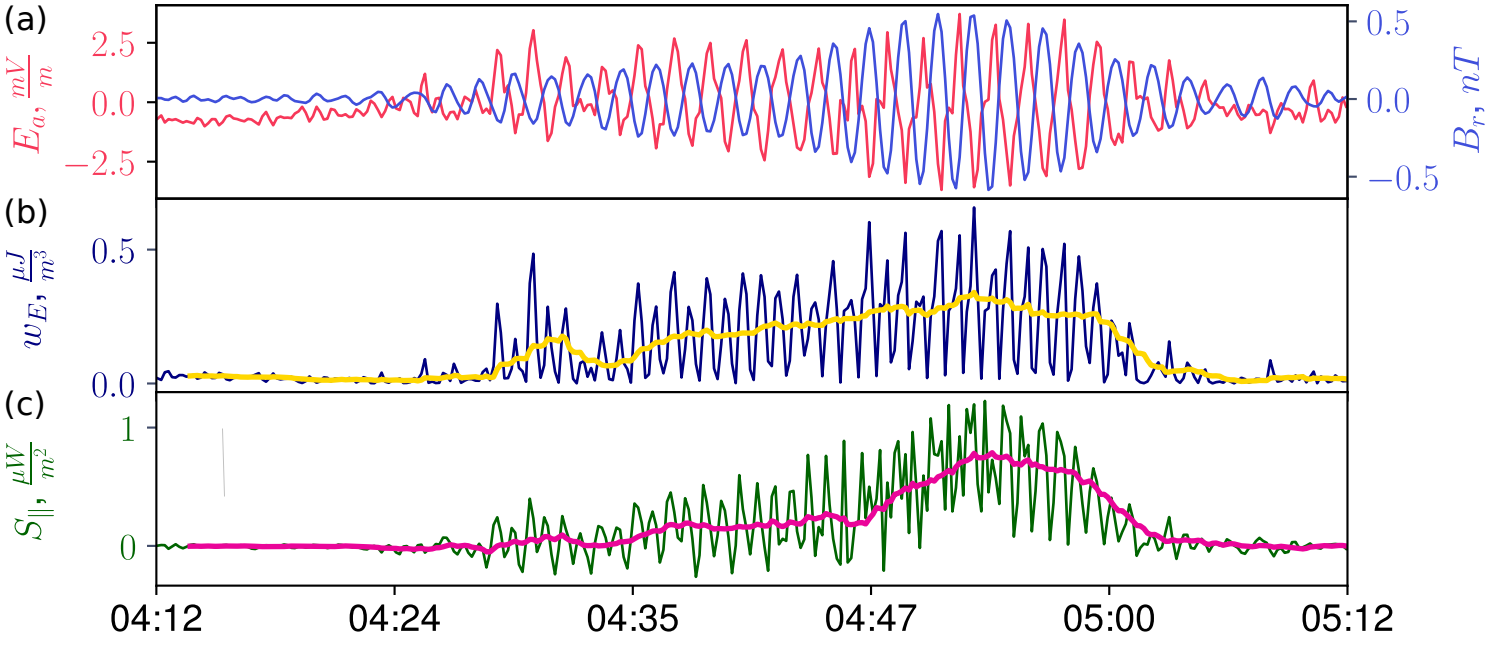
(a)
E_a, $\frac{mV}{m}$
2.5
0.0
−2.5
0.5
0.0
−0.5
B_r, nT
(b)
w_E, $\frac{\mu J}{m^3}$
0.5
0.0
(c)
$S_{\parallel}$, $\frac{\mu W}{m^2}$
1
0
04:12
04:24
04:35
04:47
05:00
05:12

Figure 2.

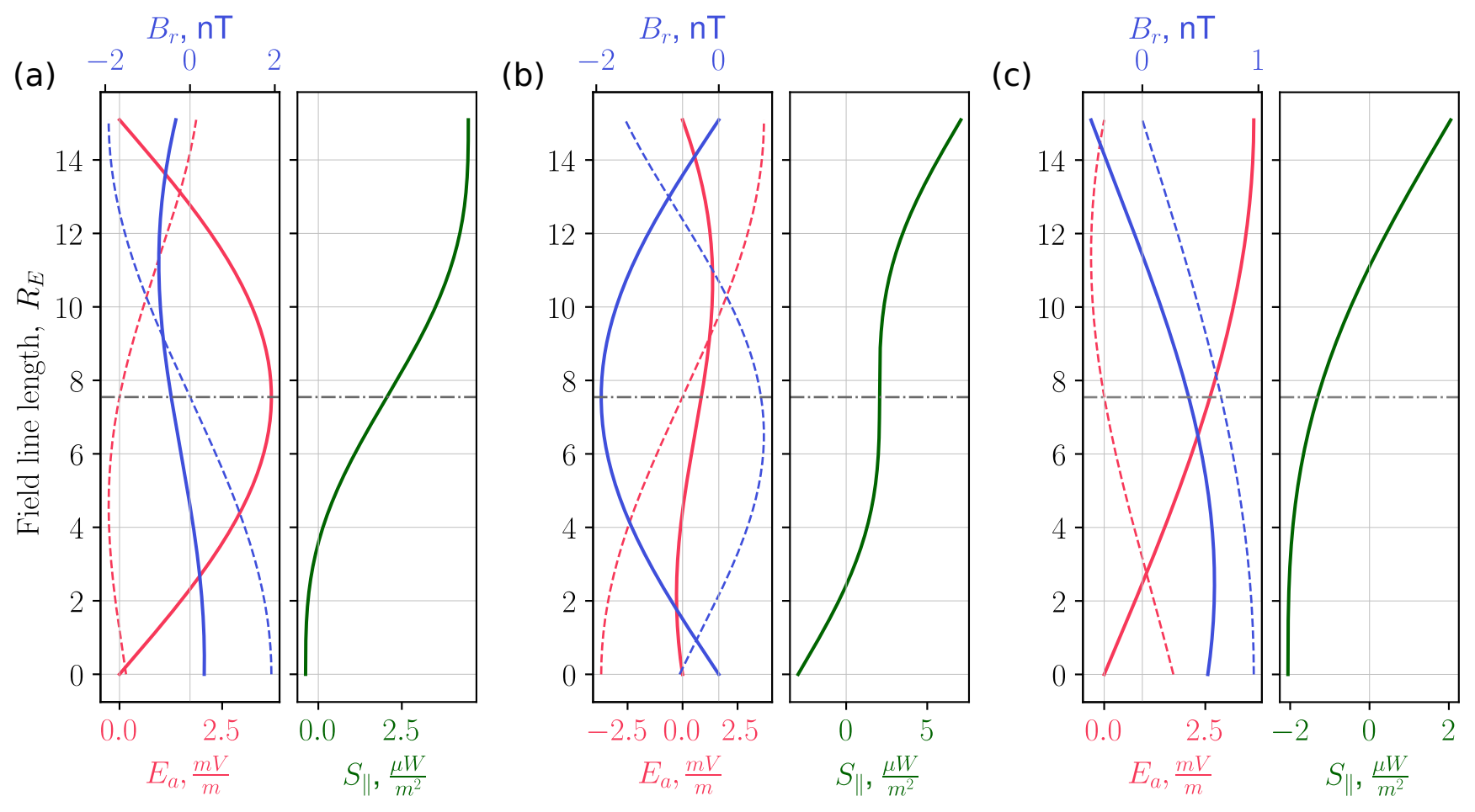
(a)
(b)
(c)
B_r, nT
Field line length, R_E
E_a, $\frac{mV}{m}$
$S_\parallel$, $\frac{\mu W}{m^2}$

Figure 3.

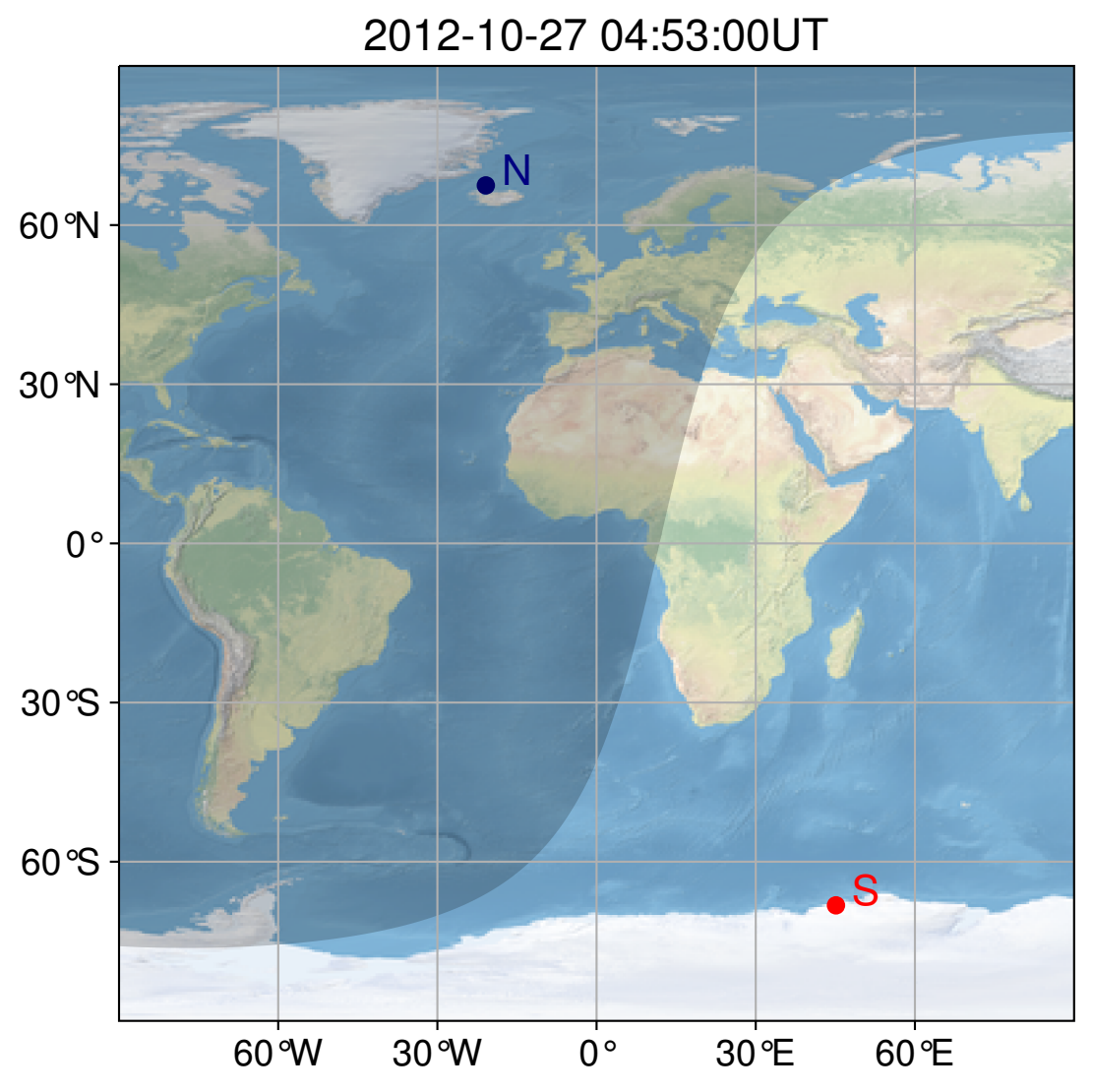
2012-10-27 04:53:00UT
N
S
60°N
30°N
0°
30°S
60°S
60°W
30°W
0°
30°E
60°E